

TOWARD A UNIFIED LIGHT CURVE MODEL FOR MULTI-WAVELENGTH OBSERVATIONS OF V1974 CYGNI (NOVA CYGNI 1992)

IZUMI HACHISU

Department of Earth Science and Astronomy, College of Arts and Sciences, University of Tokyo, Komaba,
Meguro-ku, Tokyo 153-8902, Japan
hachisu@chianti.c.u-tokyo.ac.jp

AND

MARIKO KATO

Department of Astronomy, Keio University, Hiyoshi, Kouhoku-ku, Yokohama 223-8521, Japan
mariko@educ.cc.keio.ac.jp
to appear in the Astrophysical Journal

ABSTRACT

We present a unified model for optical, ultraviolet (UV), and X-ray light curves of V1974 Cygni (Nova Cygni 1992). Based on an optically thick wind model of nova outbursts, we have calculated light curves and searched for the best fit model that is consistent with optical, UV, and X-ray observations. Our best fit model is a white dwarf (WD) of mass $1.05 M_{\odot}$ with a chemical composition of $X = 0.46$, $C + N + O = 0.15$, and $Ne = 0.05$ by mass weight. Both supersoft X-ray and continuum UV 1455 Å light curves are well reproduced. Supersoft X-rays emerged on day ~ 250 after outburst, which is naturally explained by our model: our optically thick winds cease on day 245 and supersoft X-rays emerge from self-absorption by the winds. The X-ray flux keeps a constant peak value for ~ 300 days followed by a quick decay on day ~ 600 . The duration of X-ray flat peak is well reproduced by a steady hydrogen shell burning on the WD. Optical light curve is also explained by the same model if we introduce free-free emission from optically thin ejecta. A $t^{-1.5}$ slope of the observed optical and infrared fluxes is very close to the slope of our modeled free-free light curve during the optically thick wind phase. Once the wind stops, optical and infrared fluxes should follow a t^{-3} slope, derived from a constant mass of expanding ejecta. An abrupt transition from a $t^{-1.5}$ slope to a t^{-3} slope at day ~ 200 is naturally explained by the change from the wind phase to the post-wind phase on day ~ 200 . The development of hard X-ray flux is also reasonably understood as shock-origin between the wind and the companion star. The distance to V1974 Cyg is estimated to be ~ 1.7 kpc with $E(B - V) = 0.32$ from the light curve fitting for the continuum UV 1455 Å.

Subject headings: novae, cataclysmic variables — stars: individual (V1974 Cygni) — X-rays: stars

1. INTRODUCTION

It has been widely accepted that classical novae are a thermonuclear runaway event on a mass-accreting white dwarf (WD). Characteristic properties on nova evolution have been understood from its ignition through the end of nuclear burning (e.g., Warner 1995, for a review). The next step we need is quantitative studies of individual objects. For instance, fitting of multi-wavelength light curves with theoretical models enables us to determine nova parameters. Such a work has been developed in the recurrent novae (e.g., Hachisu & Kato 2001a,b; Hachisu et al. 2000, 2003), but not yet in the classical novae except a pioneering work on V1668 Cyg (Nova Cygni 1978) by Kato (1994).

V1974 Cygni (Nova Cygni 1992) is a best example for such studies because it was extensively observed in all the wavelengths from γ -ray to radio. Among various observational data, three bands of optical, continuum ultraviolet (UV) at 1455 Å, and X-ray are used for our present study. Based on an optically thick wind model of nova outbursts (e.g., Kato & Hachisu 1994), we try to develop a unified model that yields light curves for each wavelength band. The next section introduces the light curve analysis based on our optically thick wind model. In §3, we describe light

curve fittings with X-ray, UV, and optical bands. Discussion follows in §4.

2. MODELING OF V1974 CYG

2.1. *Optically thick wind model*

After a thermonuclear runaway sets in on a mass-accreting WD, its envelope expands greatly to $R_{\text{ph}} \gtrsim 100 R_{\odot}$ and settles in a steady-state. The decay phase of nova can be followed by a sequence of steady state solutions (e.g., Kato & Hachisu 1994). Using the same method and numerical techniques as in Kato & Hachisu (1994), we have calculated theoretical light curves.

We solve a set of equations, i.e., the continuity, equation of motion, radiative diffusion, and conservation of energy, from the bottom of the hydrogen-rich envelope through the photosphere, under the condition that the solution goes through a critical point of steady-state winds. The winds are accelerated deep inside the photosphere so that they are called “optically thick winds.” We have used updated OPAL opacities (Iglesias & Rogers 1996). We simply assume that photons are emitted at the photosphere as a blackbody with the photospheric temperature of T_{ph} . Physical properties of these wind solutions have already been published (e.g., Hachisu & Kato 2001a,b, 2004;

Hachisu et al. 1996, 1999a,b, 2000, 2003; Kato 1983, 1997, 1999). It should be noticed that a large number of meshes, i.e., more than several thousands grids, are adopted for the wind solutions in an expanded stage of $R_{\text{ph}} \sim 100 R_{\odot}$.

Optically thick winds stop after a large part of the envelope is blown in the winds. The envelope settles into a hydrostatic equilibrium where its mass is decreasing in time by nuclear burning. Then we solve equation of static balance instead of equation of motion. When the nuclear burning decays, the WD enters a cooling phase, in which the luminosity is supplied with heat flow from the ash of hydrogen burning.

2.2. Multiwavelength light curves

In the optically thick wind model, a large part of the envelope is ejected continuously for a relatively long period (e.g., Kato & Hachisu 1994). After the maximum expansion of the photosphere, its photospheric radius gradually decreases keeping the total luminosity (L_{ph}) almost constant. The photospheric temperature (T_{ph}) increases in time because of $L_{\text{ph}} = 4\pi R_{\text{ph}}^2 \sigma T_{\text{ph}}^4$. The main emitting wavelength of radiation moves from optical to supersoft X-ray through UV. This causes the decrease in optical luminosity and the increase in UV. Then the UV flux reaches a maximum. Finally the supersoft X-ray flux increases after the UV flux decays. These timescales depend on WD parameters such as the WD mass and chemical composition of the envelope (Kato 1997). Thus, we can follow the development of optical, UV, and supersoft X-ray light curves by a single modeled sequence of steady wind solutions.

2.3. System parameters of optically thick wind model

The light curves of our optically thick wind model are parameterized by the WD mass (M_{WD}), the chemical composition of the envelope, and the envelope mass ($\Delta M_{\text{env},0}$) at the outburst (day 0). We have searched for the best fit model by changing these parameters, for example, in a step of $0.05 M_{\odot}$ for the WD mass, of 0.01 for hydrogen mass content, X , and of 0.05 for carbon, nitrogen, and oxygen mass content, $C + N + O$. It should be noted here that hydrogen content X and carbon, nitrogen, and oxygen content $C + N + O$ are important because they are main players in the CNO cycle but neon content is not because neon is not involved in the CNO cycle. The metal abundance of $Z = 0.02$ is adopted, in which carbon, nitrogen, oxygen, and neon are also included with the solar composition ratio. We assume neon mass content of $Ne = 0.05$ (taken from Vanlandingham et al. 2005), because neon mass content cannot be determined only from our light curve fitting.

3. LIGHT CURVE FITTING

3.1. Supersoft X-ray and UV 1455 Å fluxes

ROSAT observation clearly shows that the supersoft X-ray flux emerged on day ~ 260 after the outburst and then decayed rapidly on day ~ 600 through a plateau phase of ~ 300 days (Krautter et al. 1996). Here, we define JD 2,448,665.0 as the outburst day, 8.67 days before the optical maximum (JD 2,488,673.67). We have calculated many models, some of which are plotted in Figure 1 for

the wavelength window of 0.1 – 2.4 keV. Here, we have determined three parameters of M_{WD} , X , and $C + N + O$ by fitting three epochs with the observation, i.e., (1) when wind stops, (2) when hydrogen-burning ends, and (3) when UV 1455 Å flux reaches its maximum. We searched for the best fit model by eye.

Our calculated X-ray fluxes in Figure 1 show that the more massive the WD, the shorter the duration of X-ray flat peak, if the other two parameters are the same. This is because a stronger gravity in more massive WDs results in a smaller ignition mass. As a result, hydrogen is exhausted in a shorter period (see, e.g., Kato 1997, for X-ray turn-off time). On the other hand, if we increase hydrogen content, we have a longer duration of hydrogen burning. In this way, we choose the parameters that fit observed light curves. The best fit model is $M_{\text{WD}} = 1.05 M_{\odot}$, $X = 0.46$, $C + N + O = 0.15$, $Ne = 0.05$, and $\Delta M_{\text{env},0} \approx 1.7 \times 10^{-5} M_{\odot}$, which is denoted by a thick solid line in Figure 1. Two epochs in the best-fit model are indicated by arrows: (1) when the optically thick wind stops and (2) when the steady hydrogen-burning ends.

Thin solid lines in Figure 1 depict 1.0, 1.1, and 1.2 M_{\odot} WDs with $X = 0.35$, $C + N + O = 0.30$, and $Ne = 0.0$ while a thick solid line does the best-fit model of 1.05 M_{\odot} WD with $X = 0.46$, $C + N + O = 0.15$, and $Ne = 0.05$. To see the effect of hydrogen content, we have added two other models with the same parameters as the best-fit one except hydrogen content: $X = 0.40$ (dash-dotted line) and $X = 0.53$ (dotted line).

Figure 1 also shows that soft X-rays emerge on day ~ 250 . In our model, soft X-rays appear after the wind stops because the wind absorbs soft X-rays (e.g., Southwell et al. 1996; Hachisu & Kato 2003a,b,c). The optically thick wind stops on day 245 just the time when the supersoft X-rays emerge. After a plateau phase the X-ray flux quickly decreases as shown in Figure 1 because the hydrogen shell-burning ends on day 558.

The photospheric radius (R_{ph}), temperature (T_{ph}), luminosity (L_{ph}), and wind mass loss rate (dashed line) are plotted in Figure 2. Our results are roughly consistent with Balman et al.'s (1998) estimates for the photospheric radii and temperatures. We should place the nova at a distance of 2.2 kpc to fit our calculated X-ray flux with Balman et al.'s fluxes. This distance is longer than that derived from the UV fitting in Figure 3. See discussion.

Figure 3 depicts UV fluxes in a band of $\Delta\lambda = 20 \text{ \AA}$ wide centered at $\lambda = 1455 \text{ \AA}$, taken from Cassatella et al. (2004). The corresponding UV light curves are calculated for each model in Figure 1. Our best fitted 1.05 M_{\odot} WD model shows an excellent agreement with the observation if we place the nova at a distance of 1.7 kpc. Here we adopt an absorption law given by Seaton (1979), $A_{\lambda} = 8.3E(B - V) = 2.65$, together with an extinction of $E(B - V) = 0.32$ estimated by Chochol et al. (1997).

3.2. Optical fluxes

We cannot fit the observed visual light curve by our best fitted model or even by other models with other sets of WD mass and envelope chemical composition. Therefore, we interpret that the optical flux is dominated by free-free emission of the optically thin ejecta that exist outside the photosphere.

For the free-free emission of optically thin ejecta, optical flux can be roughly estimated as

$$F_\lambda \propto \int N_e N_i dV \propto \int_{R_{\text{ph}}}^{\infty} \frac{\dot{M}_{\text{wind}}^2}{r^4} r^2 dr \propto \frac{\dot{M}_{\text{wind}}^2}{R_{\text{ph}}} \quad (1)$$

during the optically thick wind phase, where F_λ is the flux at the wavelength λ , N_e and N_i the number densities of electron and ion, V the volume of the ejecta, \dot{M}_{wind} the wind massless rate. Here, we use the relation of $\rho_{\text{wind}} = \dot{M}_{\text{wind}}/4\pi r^2 v_{\text{wind}}$, and ρ_{wind} and v_{wind} are the density and velocity of the wind, respectively. After the wind stops, we obtain

$$F_\lambda \propto \int N_e N_i dV \propto \rho^2 V \propto \frac{M_{\text{ej}}^2}{V^2} V \propto R^{-3} \propto t^{-3}, \quad (2)$$

(e.g., Woodward et al. 1997), where ρ is the density, M_{ej} the ejecta mass (in parenthesis, if M_{ej} is constant in time), R the radius of the ejecta ($V \propto R^3$), and t the time after the outburst. Here, we substitute \dot{M}_{wind} and R_{ph} of our best fit model for those in equation(1). We cannot uniquely specify the constant in equations (1) and (2) because radiative transfer is not calculated outside the photosphere. Instead, we choose the constant to fit the light curve on day 43 denoted by A (on the *thick solid line*) and on day 245 denoted by B (on the *dashed line*) in Figure 4. These two light curves represent well the early/late parts of the observational data of AAVSO.

Woodward et al. (1997) summarized the optical and infrared (IR) observations of V1974 Cyg and concluded that $0.55\mu\text{m } V$, $1.25\mu\text{m } J$, $1.6\mu\text{m } H$, and $2.3\mu\text{m } K$ light curves all showed an abrupt transition from a $t^{-1.5}$ slope to a t^{-3} slope at day ~ 170 . This $t^{-1.5}$ slope is very close to the slope of our free-free light curve until day ~ 100 . After the wind stops, we have a slope of t^{-3} as shown in Figure 4. This transition probably occurs when the optically thick wind stops. Therefore, our model is very consistent with the temporal optical and IR observations.

4. DISCUSSION

4.1. Hard X-ray component

ROSAT observation shows that hard X-ray flux increases on day 70–100 and then decays on day 270–300. This hard component is suggested to be shock-origin between ejecta (Krautter et al. 1996). Here we present another idea that these hard X-rays are originated from a shock between the optically thick wind and the companion as described below.

V1974 Cyg is a binary system with an orbital period of $P_{\text{orb}} = 0.0812585$ days (e.g., De Young & Schmidt 1994; Retter et al. 1997). Paresce et al. (1995) and Retter et al. (1997) estimated the companion mass at $0.21 M_\odot$ from this orbital period. Using these values we obtain the separation, $a = 0.853 R_\odot$, the effective radii of each Roche lobe, $R_1^* = 0.444 R_\odot$ and $R_2^* = 0.215 R_\odot$ for the primary (WD) and the secondary component, respectively. Our optically thick wind model predicts that the companion star emerges from the WD photosphere about day 80 (for the photospheric radius, see Fig. 2).

Before day ~ 80 , the companion resides deep inside the WD photosphere and we do not detect hard X-rays. After the companion emerges from the WD photosphere, the

shock front can be directly observed. The optically thick wind stops on day 245 and we expect that the hard X-ray component decays after that. This hard X-ray flux may show orbital modulations if the inclination angle of binary is large enough. However, Chochol et al. (1997) estimated it at $i \sim 39^\circ$. For such a small inclination angle, we are able to see main parts of the shock front at any binary phase, because a bow-shock is formed off the surface of the companion (see, e.g., Shima et al. 1986) and basically optically thin to hard X-rays. Therefore, orbital modulation of hard X-ray flux is hardly observed, which is consistent with the observation (Krautter et al. 1996).

Balman et al. (1998) estimated the hydrogen column density of the hard X-ray component and concluded that it decreases, by a factor of ~ 10 , from $N_{\text{H}} \sim 10^{22.2}$ to $10^{21.3} \text{ cm}^{-2}$ between day 70 and day 260, and almost constant after that. In our optically thick wind model, the neutral hydrogen column density is given by

$$N_{\text{H}} \propto \frac{X}{m_{\text{H}}} \int_{r_{\text{s}}}^{\infty} \rho_{\text{wind}} dr \approx \frac{\dot{M}_{\text{wind}} X}{4\pi a v_{\text{wind}} m_{\text{H}}} \propto \dot{M}_{\text{wind}}, \quad (3)$$

where m_{H} is the mass of hydrogen atom, r_{s} the position of the bow-shock from the WD center, a the separation of the binary, and we roughly assume that the bow-shock front is at distance of $r_{\text{s}} = (0.5 - 0.7)a$ from the WD center. Our wind mass loss rate decreases from $\sim 10^{-5}$ to $\sim 10^{-6} M_\odot \text{ yr}^{-1}$ between day 70 and day 260 (see Fig. 2), which is very consistent with Balman et al.'s results.

4.2. WD mass and chemical composition

Several groups estimated the WD mass of V1974 Cyg. Retter et al. (1997) gave a mass of $M_{\text{WD}} = 0.75 - 1.07 M_\odot$ based on the precessing disk model of superhump phenomenon. A similar range of $0.75 - 1.1 M_\odot$ is also obtained by Paresce et al. (1995) from various empirical relations on novae. Very recently, Sala & Hernanz (2005) found the WD mass to be $0.9 M_\odot$ for 50% mixing of a solar composition envelope with a O-Ne degenerate core, or $1.0 M_\odot$ for 25% mixing, by comparing the evolutionary speed of post-wind phase of V1974 Cyg with their post-wind phase of static envelope solutions. Their values for the $1.0 M_\odot$ are roughly consistent with our results.

Vanlandingham et al. (2005) criticized Austin et al.'s (1996) results and reanalyzed chemical abundances of the ejecta from optical and UV spectra. They obtained that $\text{He} = 1.2 \pm 0.2$, $\text{C} = 0.7 \pm 0.2$, $\text{N} = 44.9 \pm 11$, $\text{O} = 12.8 \pm 7$, and $\text{Ne} = 41.5 \pm 17$ by number relative to hydrogen and relative to solar. In our notation, these correspond to $X = 0.55$, $Y = 0.25$, $C + N + O = 0.12$, $Ne = 0.06$, and $Z = 0.02$ by mass weight. The hydrogen content is a bit higher but these values are very consistent with our results.

4.3. Distance

We estimate the distance to V1974 Cyg from the UV 1455 \AA light curve fitting. The absorption at $\lambda = 1455 \text{ \AA}$ is calculated to be $A_\lambda = 8.3 E(B - V) = 2.65$ (e.g., Seaton 1979), where we adopt the absorption at the visual band, $A_V = 3.1 E(B - V) = 0.99$ (Chochol et al. 1997). Then we have a distance to the nova of $d \approx 1.7 \text{ kpc}$. For the X-ray band, Balman et al. (1998) obtained $(R_{\text{ph}}/d)^2 = (0.22 - 0.26) \times 10^{-25}$ on day 518 (corresponding to their day 511). Using $R_{\text{ph}} = 0.0115 R_\odot$ on

day 518 of our best fit model, we obtain the distance of $d = 1.6 - 1.7$ kpc, which is consistent with our distance estimation from the UV fitting. On the other hand, our X-ray flux combined with Balman et al.'s (1998) fluxes gives a rather large distance of 2.2 kpc. This difference may come from the different model parameters adopted in their atmosphere models: $1.2 M_{\odot}$ WD and $X = 0.54$, $Y = 0.21$, $Z = 0.02$, $C = 0.002$, $O = 0.103$, $N = 0.002$, and $Ne = 0.123$. Their neon mass is much higher than the observation $Ne = 0.06$ (Vanlandingham et al. 2005). Therefore we take the distance of $d = 1.7$ kpc. These distances are all within the range listed in Chochol et al.

(1997), $d = 1.3 - 3.5$ kpc with a most probable value of 1.8 kpc, derived mainly from maximum magnitude-rate of decline (MMRD) relations.

We thank A. Cassatella for providing us with their machine readable UV 1455 Å data of V1974 Cygni and also AAVSO for the visual data of V1974 Cygni. We are also grateful to the anonymous referee for useful comments to improve the manuscript. This research has been supported in part by the Grant-in-Aid for Scientific Research (16540211, 16540219) of the Japan Society for the Promotion of Science.

REFERENCES

- Austin, S. J., Wagner, R. M., Starrfield, S., Shore, S. N., Sonneborn, G., & Bertram, R. 1996, *AJ*, 111, 869
- Balman, S., Krautter, J., & Ögelman, H. 1998, *ApJ*, 499, 395
- Cassatella, A., Lamers, H. J. G. L. M., Rossi, C., Altamore, A., González-Riestra, R. 2004, *A&A*, 420, 571
- Chochol, D., Grygar, J., Pribulla, T., Komzik, R., Hric, L., & Elkin, V. 1997, *A&A*, 318, 908
- De Young, J. A., & Schmidt, R. E. 1994, *ApJ*, 431, L47
- Hachisu, I., & Kato, M. 2001a, *ApJ*, 553, L161
- Hachisu, I., & Kato, M. 2001b, *ApJ*, 558, 323
- Hachisu, I., & Kato, M. 2003a, *ApJ*, 588, 1003
- Hachisu, I., & Kato, M. 2003b, *ApJ*, 590, 445
- Hachisu, I., & Kato, M. 2003c, *ApJ*, 598, 527
- Hachisu, I., & Kato, M. 2004, *ApJ*, 612, L57
- Hachisu, I., Kato, M., Kato, T., & Matsumoto, K. 2000, *ApJ*, 528, L97
- Hachisu, I., Kato, M., & Nomoto, K. 1996, *ApJ*, 470, L97
- Hachisu, I., Kato, M., & Nomoto, K. 1999a, *ApJ*, 522, 487
- Hachisu, I., Kato, M., Nomoto, K., & Umeda, H. 1999b, *ApJ*, 519, 314
- Hachisu, I., Kato, M., & Schaefer, B. E. 2003, *ApJ*, 584, 1008
- Iglesias, C. A., & Rogers, F. J. 1996, *ApJ*, 464, 943
- Kato, M. 1983, *PASJ*, 35, 507
- Kato, M. 1994, *A&A*, 281, L49
- Kato, M. 1997, *ApJS*, 113, 121
- Kato, M. 1999, *PASJ*, 51, 525
- Kato, M., & Hachisu, I., 1994, *ApJ*, 437, 802
- Krautter, J., Ögelman, H., Starrfield, S., Wichmann, R., & Pfeffermann, E. 1996, *ApJ*, 456, 788
- Paresce, F., Livio, M., Hack, W., & Korista, K. 1995, *A&A*, 299, 823
- Retter, A., Leibowitz, E. M., & Ofek, E. O. 1997, *MNRAS*, 286, 745
- Sala, G., & Hernanz, M. 2005, *A&A*, in press (astro-ph/0502092)
- Seaton, M. J. 1979, *MNRAS*, 187, 73
- Shima, E., Matsuda, T., & Inaguchi, T. 1986, *MNRAS*, 221, 687
- Southwell, K. A., Livio, M., Charles, P. A., O'Donoghue, D., & Sutherland, W. J. 1996, *ApJ*, 470, 1065
- Vanlandingham, K. M., Schwarz, G.J., Shore, S.N., Starrfield, S., & Wagner, R.M. 2005, *ApJ*, submitted (astro-ph/0501648)
- Warner, B. 1995, *Cataclysmic variable stars*, Cambridge, Cambridge University Press
- Woodward, C. E., Gehrz, R. D., Jones, T. J., Lawrence, G. F., & Skrutskie, M. F. 1997, *ApJ*, 477, 817

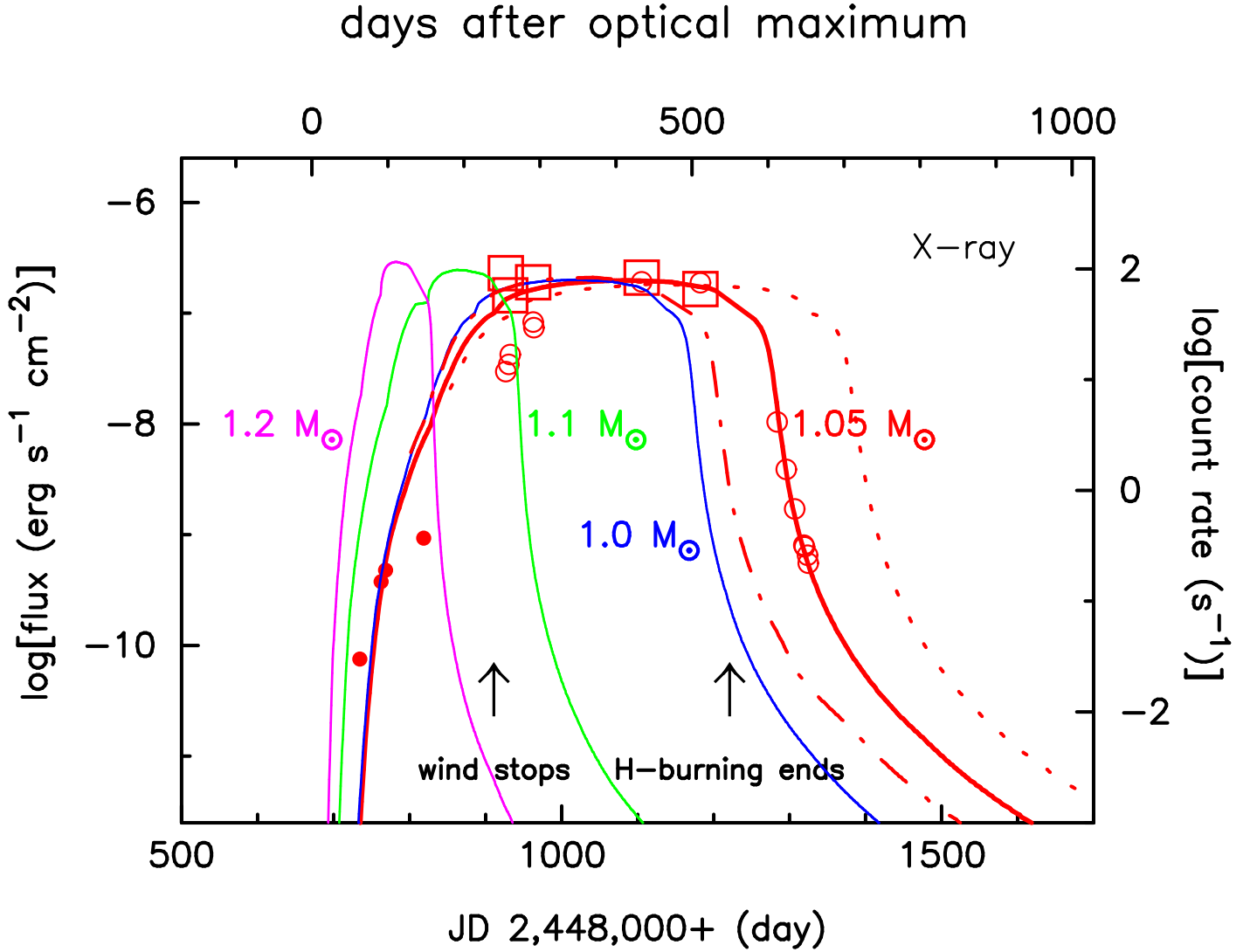


FIG. 1.— Calculated X-ray fluxes (0.1 – 2.4 keV) from white dwarf (WD) photospheres are plotted against time for various WD masses and chemical compositions together with *ROSAT* observation count rates (*open and filled circles*: taken from Krautter et al. 1996). *Open circles*: dominated by soft X-rays. *Filled circles*: dominated by hard X-rays. *Open squares*: corrected X-ray fluxes (Balman et al. 1998). The distance is assumed to be 2.2 kpc (see Discussion). The epoch of the optical maximum corresponds to JD 2,448,673.67, which is 8.67 days after the outburst. *Thin solid lines*: 1.0 M_{\odot} , 1.1 M_{\odot} , and 1.2 M_{\odot} WDs with the envelope composition of $X = 0.35$, $C + N + O = 0.30$, and $Ne = 0.0$. *Thick solid line*: the best-fit model of 1.05 M_{\odot} WD with $X = 0.46$, $C + N + O = 0.15$, and $Ne = 0.05$. Two other models are depicted for the same parameters as the best-fit one except hydrogen content, $X = 0.40$ (*dash-dotted line*) and $X = 0.53$ (*dotted line*). Two epochs of the best-fit model are indicated by arrows.

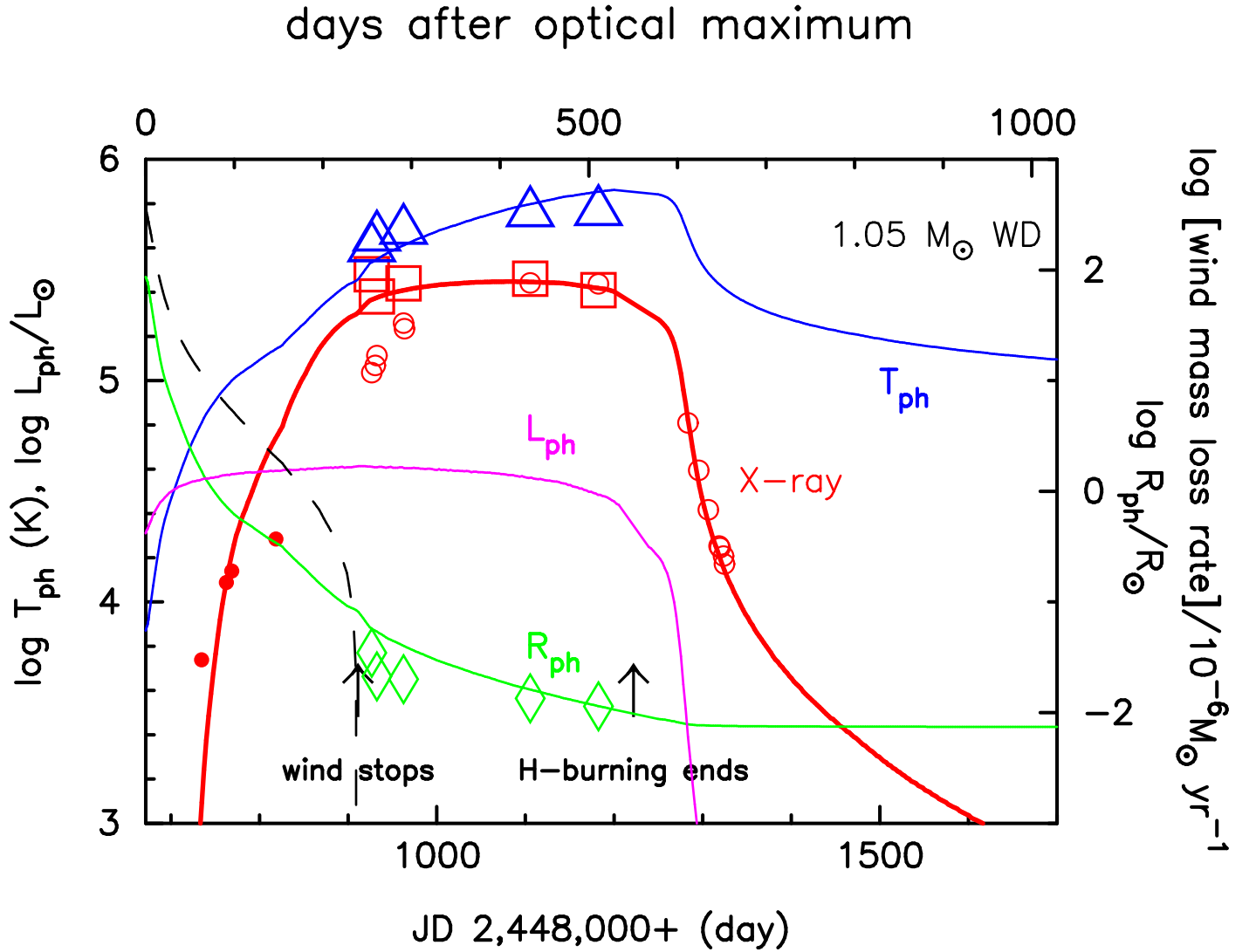


FIG. 2.— Wind mass loss rate (*dashed line*), photospheric temperature (T_{ph}), photospheric radius (R_{ph}), photospheric luminosity (L_{ph}), and X-ray flux (*thick solid line*) of the best fit model ($M_{\text{WD}} = 1.05 M_{\odot}$, $X = 0.46$, $C + N + O = 0.15$, and $Ne = 0.05$). X-ray fluxes (*Open squares*), photospheric temperatures (*Open triangles*), and photospheric radii (*Open diamonds*). These are taken from Balman et al. (1998). Here, photospheric radii are calculated from $A_1 \equiv (R_{\text{ph}}/d)^2$ in Balman et al.’s Table 1 with the distance of $d = 1.7$ kpc. *Open and filled circles*: the same X-ray count rates as in Fig. 1. See discussion for more details.

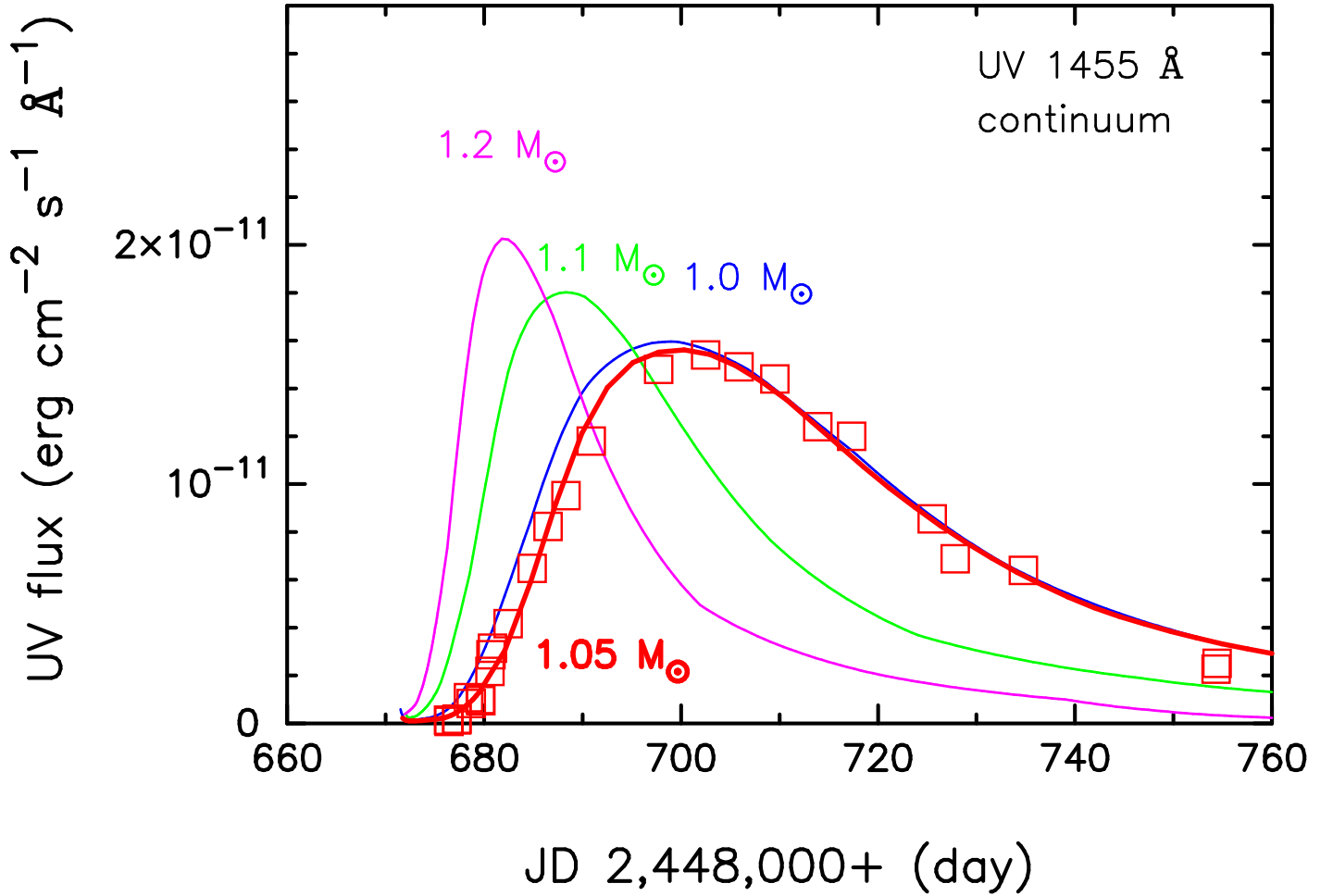


FIG. 3.— Calculated UV ($\lambda = 1455 \text{ \AA}$) fluxes are plotted together with the *IUE* observations (*open square*: taken from Cassatella et al. 2004). These curves correspond to the four models (*solid lines*) in Fig. 1. The distance of $d = 1.7 \text{ kpc}$ is assumed. Here we use Seaton's (1979) absorption law of $A_{\lambda} = 8.3 E(B - V) = 2.65$ with an extinction of $E(B - V) = 0.32$ (Chochol et al. 1997).

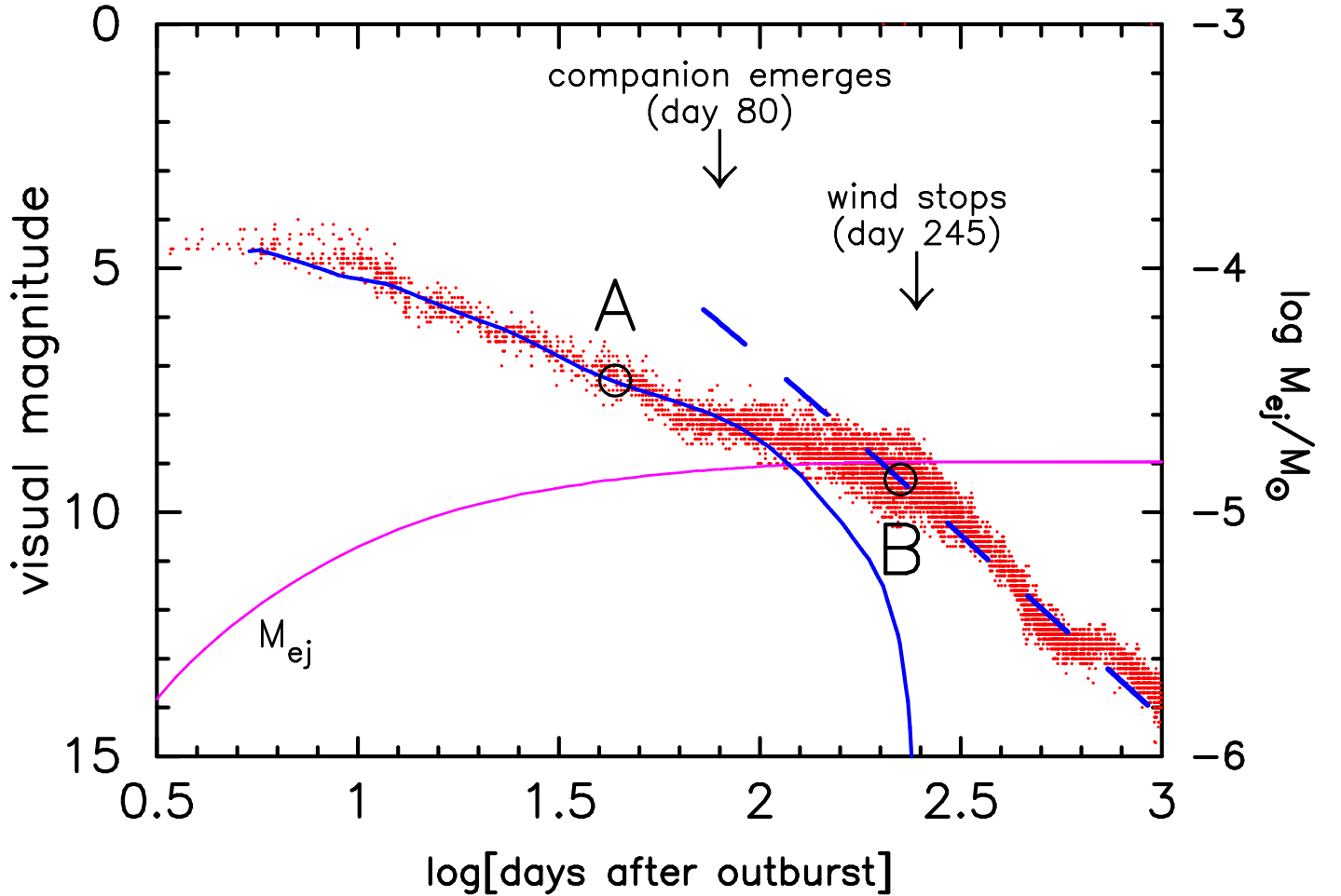


FIG. 4.— *Thick solid line:* visual magnitude of free-free emission from the optically thin ejecta, based on equation (1): scaled to fit at day 43 (point A). The flux decays with a slope of $\sim t^{-1.5}$ until day ~ 100 . *Dashed line:* free-free emission with a slope of $\sim t^{-3}$ after the wind stops: scaled to fit at day 224 (point B). *Thin solid line:* ejected mass (M_{ej}) from the WD by the optically thick winds. Here, we assume JD 2,448,665.0 as the date of outburst. *Small dots:* observational magnitudes taken from AAVSO archive. Two epochs of the nova outburst are indicated by arrows: the companion emerges from the WD photosphere and the optically thick nova wind stops.